Resolution and contrast reduction

Ralph E. Shuping

Medical Physics Branch Division of Electronic Products, Bureau of Radiological Health, Food and Drug Administration, Department of Health, Education, and Welfare, 5600 Fishers Lane, Rockville, Maryland 20857

Philip F. Judy

Department of Radiology, Harvard Medical School and Peter Bent Brigham Hospital, 25 Shattuck Street, Boston, Massachusetts 02115

(Received 17 April 1978; accepted for publication 30 August 1978)

Lack of resolution (unsharpness) can reduce contrast in diagnostic radiography if the proper conditions of magnification and unsharpness are met. To describe this phenomenon, a modification of the contrast reduction factor (CRF) was introduced which used the response function of a semi-opaque edge to predict contrast reduction for small bar-shaped objects. To predict CRF, unsharpness is employed as a single-term description of resolution and is obtained experimentally from the edge response function. The unsharpness term is defined as the distance over which the response goes from 16.5% to 83.5% of the maximum. Measured and predicted CRFs were compared and the CRF concept was found to be an excellent predictor of contrast reduction. The individual components of unsharpness were determined experimentally and the sum-of-squares rule predicted adequately their combination. Three methods to measure unsharpness were compared: (a) the ICRU prescription using pinhole radiographs of the focal spot, (b) one-dimensional integration of the focal-spot pinhole radiograph, and (c) the unsharpness term produced by a semi-opaque edge. The latter two were measured using a microdensitometer.

I. INTRODUCTION

A. Background

Unsharpness, a single-parameter descriptor of resolution, was developed and used to express small-object contrast through the use of the contrast reduction factor (CRF). Resolution is a general term indicating the ability of the imaging system to reproduce a spatial variation in x-ray intensity while unsharpness, as defined here, is a single parameter description of resolution. It is realized that a single parameter is inadequate to describe fully the consequences of resolution in an x-ray imaging system, but such a description can be of value in many situations. This paper describes the relationship between several single parameter descriptions of resolution that have been proposed, formally[1] (ICRU 10f) and informally.

Resolution impacts upon the contrast of small objects and may result in diminution of contrast. To express this, the unsharpness term was used to predict contrast of small objects. Small-object contrast is of importance in diagnostic radiology because of the size of many important anatomical structures. Examples are small blood vessels in contrast radiography and calcium specks in mammography. Prediction of contrast reduction was investigated in terms of a one dimensional contrast reduction factor developed for high density bars.

Geometry, the image receptor, and motion determine the resolution of a radiographic system.[2] Resolution has been rigorously described using the modulation transfer function (MTF)[3,4] and the square-wave response function (SWRF).[5] Differentiation of the edge-response function into the line spread function was used by Schwenker[6] to obtain the MTF.

In this paper, resolution was measured from the intensity distribution produced by an edge. Unsharpness was defined as the distance between the 16.5%–83.5% intensity points on the edge trace. Intensity was obtained from optical density by use of the film or film–screen characteristic curve.

Contrast[7] is a measure of the difference in signal levels between two areas within an image, the area comprising the shadow of an object one desires to visualize, and the area surrounding the object's shadow. Subject contrast (SC) is the ratio of the photon-number difference to the photon number in the surrounds and radiographic contrast (RC) is the optical-density difference.

B. Unsharpnesses

The appropriate method (sum-of-squares rule) to combine the components of resolution was discussed by Wagner *et al.*[8] and by Spiegler and Norman,[9] who cited the central limit theorem. Birch[10] earlier concluded that, for a multicomponent system with as little as three components of resolution, the system spread function will be in a form that is approximated well by a Gaussian distribution even when the individual components are not.

An edge spread function (ESF) is the integral of a line spread function (LSF). If the LSF is Gaussian, the ESF can be represented by the integrated normal function with the unsharpness descriptor given by the distance (similar in concept to the standard deviation of a statistical process) over which the ordinate goes from 0.165 to 0.835, over a scale of zero to unity (Fig. 1). Even if the distribution is not normal

 0094-2405/78/0506-0491$01.20

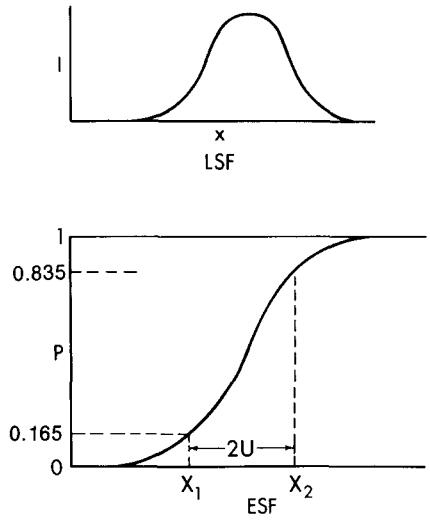

FIG. 1. A line spread function and its integration into an edge spread function.

in shape, this prescription is an attractive method to specify unsharpness because individual unsharpnesses can be measured readily.

The sum-of-squares rule applied to unsharpness is expressed as

$$U_t^2 = U_g^2 + U_m^2 + U_i^2. \tag{1a}$$

Where

$$U_i = I, \tag{1b}$$

$$U_g = G(M - 1), \tag{1c}$$

and

$$U_m = 0.67\, V_0\, M\, t. \tag{1d}$$

The symbols (U_t, U_m, U_g, and U_i) mean total, motion, geometric, and image receptor unsharpness, respectively, in the image plane.

G and I are unsharpness values obtained as prescribed above. V_0 is the object velocity, t is the exposure time, and M is the magnification factor. This analysis assumes a constant velocity and, to be consistent with the other terms, the value of U_m is obtained using the factor 0.67.

Unsharpness (G) determined by this method may be used to express focal-spot size. Ardran and Crookes[11] used a ground tungsten knife edge to produce an image and used this edge to determine focal-spot size. They reported good correlation between the knife-edge results and focal-spot dimensions determined with a pinhole camera and the ICRU[1] prescription.

C. Contrast reduction factor

The effect of resolution on small-object contrast has been considered by Haus and Rossmann,[12] Sandor and Adams,[13] and Sandor *et al.*[14] They predicted contrast reduction in terms of convolution of the LSF of the system with the photon intensity distribution transmitted through the test object. Wagner[15] expressed contrast reduction in terms of the sampling aperture of the system and used the term contrast reduction factor (CRF) to describe this effect. We employed the CRF as a one-dimensional parameter to predict contrast reduction at the center of the image but not to predict the envelope of the distribution.

The CRF was predicted assuming that the normal function describes the LSF of the total system. The total unsharpness U_t was defined to be analogous to the standard deviation. The CRF is then described by the integral of the normal function. This function $P(x')$ is tabulated[16] in terms of x':

$$x' = (x - \mu)/U_t. \tag{2}$$

x' is the distance that x is from the edge in units of unsharpness. μ is the offset of the edge from an arbitrary origin. The value of the ESF at the center of an image of a bar object (width equal to W) is used to estimate the CRF. The CRF is the ratio of the contrast of a small object (comparable in width to the unsharpness) to the contrast of a large bar.

CRF estimated assuming a normal LSF is then:

$$\text{CRF} = [2P(W/2U_t) - 1]. \tag{3}$$

Figure 2 illustrates the large area, resolution limited, and edge contrasts. The CRF is derived in terms of intensity and is used to determine intensity reduction at the center of the image. The product of the CRF by the photon intensity at the center yields the reduced signal, from which one can calculate radiographic contrast.

II. METHOD AND MATERIALS

A. Materials

The x-ray unit was a specially built single-phase full-wave rectified generator having minimum and maximum ratings of 20–150 kVp and a current rating of 0–250 mA, both continuously variable. The x-ray tube was mounted on an optical bench and has either a 1.0 or 2.0 mm nominal focal spot and approximately 0.7-mm-Al inherent filtration.

A cassette with 3.2-mm-thick bakelite face was used to support the film–screen combination (TF-2, RP film) or film (RP) on the optical bench. A holder was constructed and fixed to a slide so that the receptor could be positioned accurately on the bench. The experimental configuration was illustrated in a previous publication.[17]

Processor chemistry, time, and temperature were well controlled during the study. This was necessary to enable use of the characteristic curve of the image receptor system to obtain intensity. An Optronics Specscan 3000 microdensi-

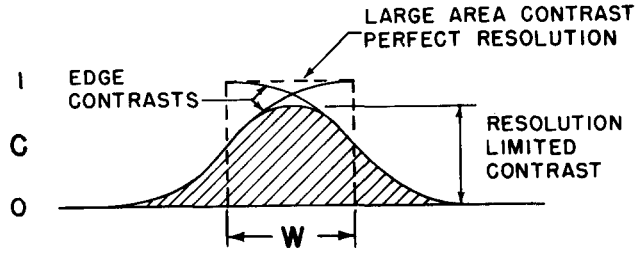

FIG. 2. The contrast reduction relationship. W is the width of the test object. The edge of the object is denoted by the vertical dotted lines and the cross-hatched area is the resultant image of the rectangular object. Given no unsharpness, the image would occupy the area within the dotted lines. The center of the normal distribution function is placed on the edge of the perfect image (dotted line).

tometer with a 10 × 1100-μm scanning slit was used to determine optical-density profiles.

B. Experimental measurement techniques

1. Determination of unsharpness

A variation of the edge method was used to quantify unsharpness. The edge was a 1.5-mm-Al milled sheet, oriented with the edge on the central ray of the x-ray beam. This thickness yielded film contrast of approximately 0.35 OD units for an 80 kVp, 2.85-mm Al-HVL beam with approximately 3.2-mm Al-equivalent total filter in the beam. Placing the edge in contact with the image receptor eliminated geometric unsharpness; the unsharpness recorded on the film was due to the screen–film only.

Geometric unsharpness was determined by magnifying the edge using directly exposed RP film. The edges were scanned to obtain optical density and intensity profiles and, from the latter, the unsharpness.

Sources of unsharpness were combined experimentally by substituting the film–screen system for direct exposure film and producing magnified images of the edge. Total unsharpness was calculated using Eq. (1) and the experimentally determined unsharpness values. Optical density was transformed to intensity by use of the appropriate characteristic curve.

2. Small object contrast

Small object contrast was evaluated using a series of repeating bar patterns,[18] ranging from 20 lp/mm (0.025-mm wide) to 0.5 lp/mm (1-mm wide). Exposure was at 80 kVp with the plate in contact and at two magnifications. Two focal spots sizes were used. Each set of parallel bars has a single bar projecting from the series to provide a measure of contrast. Images of this bar were used to evaluate loss of contrast due to geometric and image receptor unsharpness.

Contrast was defined by the relationship:

$$C = \Delta I/I, \tag{5}$$

where I was the intensity near the test object and ΔI the difference in intensities between the test object and the surrounding area.

The contrasts of the test objects were compared by

$$C_1/C_r = (\Delta I_1/\Delta I_r)(I_r/I_1). \tag{6}$$

In this equation, C_1 and C_r are the contrasts of the test and reference objects, ΔI_1 and ΔI_r are the contrast differences, and I_1 and I_r are the intensities associated with each. Multiplication by the normalizing ratio (I_r/I_1) is necessary because the set of test objects is rather large and intensity variation over the set was observed.

3. Focal-spot unsharpness and other measures of focal-spot size

Focal-spot unsharpness determined using the edge trace method is also a measure of focal-spot size. To complement the edge measurements of focal-spot unsharpness (and size), pinhole radiographs using fine-grain direct-exposure film were made as a function of kVp and mA. Focal-spot sizes were determined using the microdensitometer to perform one-dimensional integrations parallel to the double bands, thus simulating an edge exposure. The length of the microdensitometer scanning slit (1.1 mm) was less than the size of the smallest image, and multiple scans were done to cover the entire width of the image. The densities were summed and averaged and base plus fog density was subtracted. The gross optical density was always less than 1.2 to ensure a linear relationship between exposure and optical density.

The ICRU prescription, a standard method of focal-spot-size determination, calls for estimating the maximum dimensions of the focal spot under 10 power magnification and multiplying the resultant value by 0.7.

III. RESULTS

A. Small object contrast

Experimental and calculated values of CRF are presented [Figs. 3(a–e)] for a TF-2 screen, RP film combination. Experimental results are presented with the bars oriented both parallel and perpendicular to the anode–cathode axis of the tube. Calculated results (solid lines) illustrate the agreement obtained at each magnification. Screen–film unsharpness (U_i) and focal-spot unsharpness (U_g) were evaluated experimentally. CRF was evaluated using Eq. (3), P being calculated using experimental values of U_g and U_i, the width of the test object in the film plane, and tabulated data for each value of $P(W/2U_t)$.

B. Unsharpness

The edge trace method was used to determine the unsharpness of several screens and the unsharpness of the focal spot at several magnifications. Using the edge trace method, total unsharpness was confirmed experimentally to be represented adequately by the square root of the sum of squares of the individual unsharpnesses. The discrepancy between calculated and measured values of unsharpnesses was found to be approximately 6% at a magnification of 2. Motion was not considered in this analysis. Had it been, agreement between experiment and calculation would have been improved by the addition of another component of unsharpness. Unsharpness of the U. S. Radium TF-2 screen was found to be 0.19 mm, while the values for several other screens were UD-2, 0.12; T-2, 0.16; and STF-2, 0.22 mm. These values are in terms of I, which corresponds to one standard deviation of a normal distribution.

C. Focal-spot unsharpness

Focal-spot unsharpnesses were estimated using the edge trace and one-dimensional integration of a pinhole radiograph. These were compared to unsharpness (or size) obtained with the ICRU technique. Results obtained with these three methods are presented in Table I. The values of focal-spot size listed under the edge trace and integration methods are the unsharpness values G determined from the edge trace. The values in brackets are the result of multiplying the unsharpness value by the factor 3.5 to estimate focal-spot size.

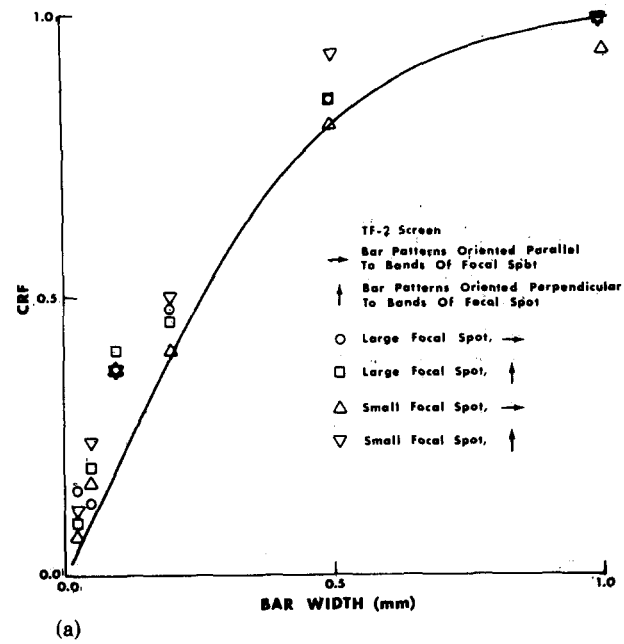

(a)

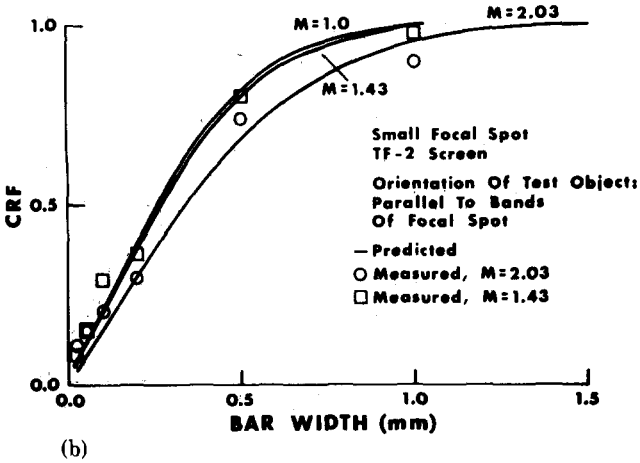

(b)

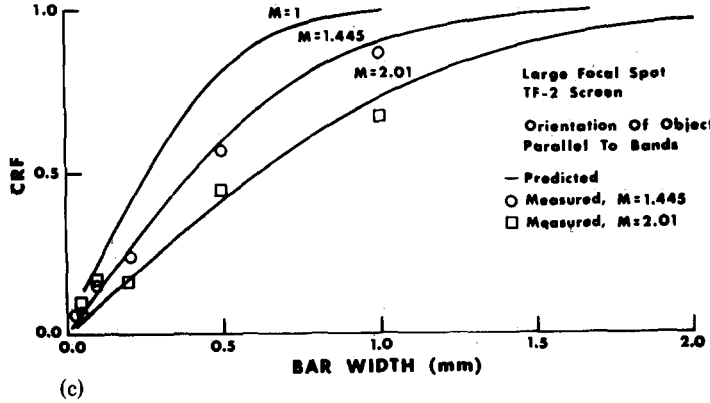

(c)

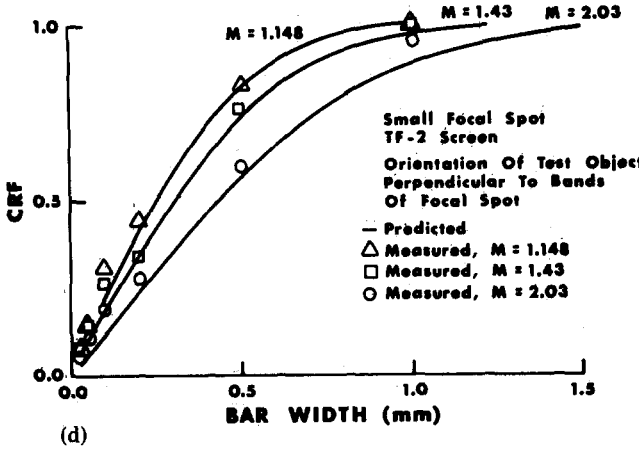

(d)

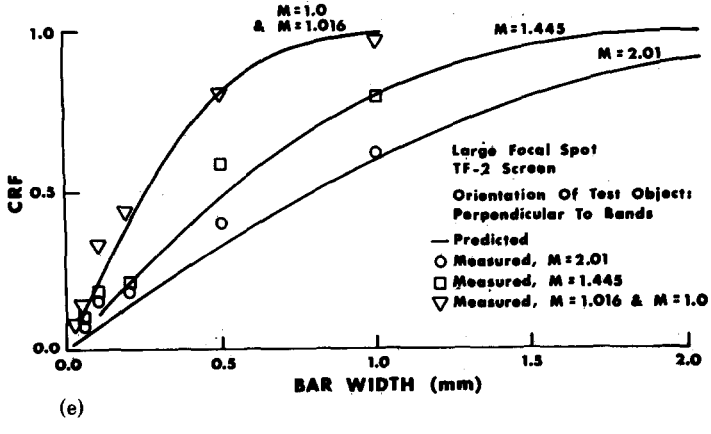

(e)

FIG. 3. (a) The contrast reduction factor (CRF) is presented as a function of bar width for two orientations and two focal-spots. The test pattern is in contact with the cassette ($M = 1$). Calculated CRF is represented in this figure by one entry only (the line), since for unity magnification only the screen–film unsharpness factor affects the CRF. (b) Comparison of the CRF predicted and measured for a small focal-spot with parallel orientation of the bars to the focal-spot, and at two magnifications. The predicted value for unity magnification is included for comparison. (c) Comparison of the CRF predicted and measured for the large focal-spot, parallel orientation and two magnifications. The predicted value of CRF for unity magnification is presented for comparison. (d) Comparison of the CRF predicted and measured for the small focal-spot with perpendicular orientation of the bars to the bands of the focal spot. Unity magnification nearly coincided with the prediction for M = 1.148 and was not presented. (e) Comparison of the CRF predicted and measured for the large focal-spot with perpendicular orientation of the bars to the bands of the focal-spot and at three magnifications. The predicted value of CRF for unity magnification is presented and was found to coincide with the predicted value for $M = 1.016$.

TABLE I. Comparison of measurement of focal-spot unsharpness (or size) by the edge trace, pinhole radiograph integration, and ICRU methods. One dimension only, scan and measurement done perpendicular to double bands of the focal spot.

			Focal-spot size (mm) determined by:		
	kVp	mA	Edge trace	Integration of pinhole radiograph[a]	ICRU method
Large	100	250	0.87		
		150	0.83(2.91)[b]	0.77(2.71)[b]	1.97(2.81)[c]
		50	0.80		
Small		100	0.46		
		50	0.45		
Fluoro		5	0.53		
Large	80	250	0.83(2.92)	0.78(2.75)	1.97(2.81
		150	0.84(2.96)	0.77(2.71)	2.04(2.91)
		50	0.80		
Small		100	0.45(1.59)	0.40(1.38)	1.20(1.71)
		50	0.46(1.63)	0.41(1.44)	1.34(1.91)
Fluoro		5	0.52		
Large	60	250	0.90(3.15)	0.82(2.87)	2.04(2.91)
		150	0.84(2.96)	0.79(2.77)	1.97(2.81)
		50	0.81(2.84)	0.75(2.64)	1.90(2.71)
Small		100	0.46		
		50	0.45		
Fluoro		5	0.51(1.79)	0.45(1.59)	1.27(1.81)

[a]Integration done with the slit across the double bands of the focal-spot.

[b]The values tabulated in the edge trace and integration columns are in terms of G. Multiplying G by 3.5 yields the value in brackets.

[c]The values tabulated were obtained by the ICRU prescription. The bracketed values are the measured sizes of the focal-spot prior to multiplication by 0.7.

IV. DISCUSSION AND CONCLUSION

Doi and Sayanagi[19] fitted one-dimensional focal-spot data with a Gaussian model and reported the focal-spot width to be represented by 3 standard deviations of the Gaussian. Wagner *et al.*[8] used the equivalent passband to calculate the average blur of the Gaussian smear of a focal spot. The resultant blur diameter was 3.5 standard deviations for a one-dimensional calculation. Doi and Rossmann[20] introduced the root-mean-square (RMS) equivalent focal spot, which is the product of the RMS of the focal-spot LSF by the factor 3.5.

The factor 3.5 was applied to the edge trace and integration data; the resultant estimates of focal-spot size are presented in Table I in brackets. Good agreement was obtained between estimates of focal-spot size made by visual observation and the edge trace method.

The factor 3.5 was also applied to the four screen unsharpness values quoted previously. The results were consistent, both in magnitude and rank, with unsharpness data obtained by Burgess[21] from focal-spot MTF values. Consequently, the edge trace method yields estimates of screen unsharpness I and focal spot unsharpness G that are consistent with independent measurements of unsharpness.

The discrepancy (6%–12%) observed between the values obtained by edge trace and by pinhole radiograph integration is to be expected if the edge is misaligned. Calculations indicate that the thickness of the edge (1.5 mm) used to generate the edge trace data and a misalignment of 5° from the central ray would produce an approximate smearing of 8% in the edge profile. This much misalignment was possible with the experimental arrangement used to evaluate focal-spot unsharpness; the discrepancy is of this magnitude.

A second source of error was the use of a long slit (1000 μm) to integrate density perpendicular to the direction of the trace. The proper method to integrate density of the image is to use a small aperture over which density does not vary significantly, the average density being obtained from a large number of scans across the image.

A 20 × 20-μm aperture was used to scan an image of the small focal spot. The unsharpness value obtained using this aperture was approximately 6% larger than the value obtained with the long slit. Therefore the entries in Table I determined by integration of the pinhole image are somewhat lower in value than they would be if integrated with a small aperture. The difference results from the logarithmic relationship between transmission and density; the density resulting from the average of two transmissions is not equal to the average of the two densities. This inequality is small for small differences in density and increases with density difference.

These two sources of error account for the observed discrepancy; edge misalignment should yield larger and the integration method used should yield smaller unsharpness values than truly exist.

The 2-mm focal spot was found to change with mA (found to bloom) by approximately 10%. No significant increase was observed for the 1-mm spot.

The edge trace method imposes a small heat load on the x-ray tube, while the ICRU method requires a substantial heat load depending on the size of the pinhole used to produce

the radiograph. The edge method is simple and effective if one has the facilities to evaluate the image densitometrically.

The unsharpness descriptor of resolution introduced in this paper is a practical method to quantify both focal-spot size and focal-spot and image-receptor unsharpness, and provides the basis for a practical and accurate method of predicting contrast reduction. An advantage is its simplicity compared to more complex descriptors. It is easily obtained using an edge and requires no more sophisticated equipment for extraction of data than do the more complex methods. To obtain valid results, it is not necessary to define unsharpness with the parameter detailed here. Other advantages of the unsharpness approach are its reproducibility and the exclusion of value judgements associated with the ICRU method.

Experimentally, the sum-of-squares method of combining unsharpnesses was found to be valid. Using this approach, it is logical to define unsharpness as if it were equivalent to the standard deviation of a normal (statistical) distribution.

Motion is a factor to be considered in many radiographic studies and will have an impact on resolution if not controlled by means of shortened exposure time. As previously demonstrated, resolution will reduce contrast if the appropriate conditions of magnification and unsharpness are encountered. Motion unsharpness should not dominate total unsharpness, but ideally should be comparable in magnitude to the combined unsharpness of the other components of the system.

The concepts developed regarding unsharpness can be used to predict and control effects of multiple unsharpnesses upon resolution. An example is the use of faster or slower screens and the unsharpness parameters associated with those particular screens. If one must reduce motion unsharpness, use of a faster screen will accomplish this goal but at the expense of increased screen unsharpness.

The CRF was demonstrated to be a reasonable predictor of contrast reduction for small bar-shaped objects [Figs. 3(a–e)], and was simply calculated from the components of unsharpness. The CRF was developed in terms of an edge which is long compared with the magnitude of the unsharpness term; it should be most applicable to studies of objects having this shape, such as blood vessels containing contrast media or calcium deposits.

ACKNOWLEDGMENT

This work was supported in part by USPHS grant GM18674.

[1] *Methods of Evaluating Radiological Equipment and Materials,* ICRU Rep. 10f (ICRU, Washington, DC, 1962).
[2] W. J. Meredith and J. B. Massey, *Fundamental Physics of Radiology,* 2nd Ed. (Williams and Wilkins, Baltimore, MD, 1972).
[3] R. H. Morgan, Am. J. Roentgenol. **88,** 175 (1962).
[4] K. Rossman, Am. J. Roentgenol. **90,** 178 (1963).
[5] G. Lubberts, Am. J. Roentgenol. **91,** 650 (1969).
[6] R. P. Schwenker, in *Image 72, 25th Annual Conferences* (Soc. of Photo. Scientists and Engineers, Washington, DC), May 1972.
[7] H. E. Seemann, Am. J. Roentgenol. **80,** 112 (1958).
[8] R. F. Wagner, K. E. Weaver, E. W. Denny, and R. G. Bostrum, Med. Phys. **1,** 11 (1974).
[9] P. Spiegler and A. Norman, Phys. Med. Biol. **18,** 884 (1973).
[10] K. G. Birch, Survey of OTF Based on Criteria Used in the Specification of Image Quality, Natl. Phys. Lab. Teddington, England, 1969 (Clearinghouse, Springfield, VA, No. 70-21982).
[11] G. M. Ardran and H. E. Crooks, Brit. J. Radiol. **44,** 625 (1971).
[12] A. G. Haus and K. Rossmann, Radiol. **106,** 127 (1973).
[13] T. Sandor and D. F. Adams, Radiol. **109,** 195 (1973).
[14] T. Sandor, D. F. Adams, P. G. Herman, H. Eisenberg, and H. L. Abrams, Am. J. Roentgenol. **120,** 916 (1974).
[15] R. F. Wagner, Med Phys. **4,** 279 (1977).
[16] R. S. Burrington, *Handbook of Mathematical Tables and Formulas* (Handbook Publishers, Inc., Sandusky, OH, 1956).
[17] R. E. Shuping and P. F. Judy, Med. Phys. **4,** 239 (1977).
[18] B. A. Hollander, S. K. Hilal, and W. B. Seaman, Radiol. **103,** 667 (1972).
[19] K. Doi and K. Sayanagi, Jap. J. Appl. Phys. **9,** 834 (1970).
[20] K. Doi. and K. Rossmann, in *Application of Optical Instrumentation in Medicine III* (Society of Photo-optical Instrumentation Engineers, Palos Verdes Estates, CA, 1974).
[21] A. E. Burgess, Med. Phys. **5,** 199 (1978).